Sound power and sound energy measurements using an ellipsoidal measurement surface

Edward Zechmann[1]
National institute for Occupational Safety and Health
1090 Tusculum Avenue

ABSTRACT

Sound power and sound energy measurements characterize the noise emitted by noise sources. The advancement of these measurements could include the ellipsoidal measurement surface. Sound power measurements using ISO 3744 and 3745 are simulated in a free field using an acoustic far-field approximation of the intensity integrated over an enveloping measurement surface. Sound power and sound energy measurements generally use a hemispherical, parallelepiped, or cylindrical measurement surface. Those measurement surfaces have limitations and assume that the microphone positions lie on the measurement surface often in preferred positions. An alternative approach is to choose microphone positions that optimally satisfy the assumptions of the measurement. The measurement surface would then be fit to the chosen microphone positions. Regression methodologies are available for fitting ellipsoids. The number of microphone positions can be as few as three to fit an ellipsoid. An ellipsoidal measurement surface can abut zero, one, two, or three orthogonal reflecting planes. Correction equations for the microphone locations and the angle errors for the microphone orientation and wave propagation direction are described. This paper will present simulations of sound power and K_2 corrections for environmental reflections for measurement surfaces used in ISO 3745 and other measurement surfaces.

1. "BUY QUIET" REQUIRES SOUND ENERGY MEASUREMENTS

Experts performing noise assessments need the ability to make reasonably quick and accurate sound energy (joules) measurements to support "Buy Quiet" as a global solution to excessive noise. Sound energy takes productivity into consideration which is important for practical comparison of power tools. The safety procurement standard SAE AS6228 considers all safety health and cost factors influencing a purchasing decision [1]. The standard could benefit from a quicker and easier way to make sound energy measurements. Currently sound power measurements are made using hemispherical, parallelepiped, or cylindrical measurement surfaces which have certain limitations and often use preferred microphone positions [2-4]. An alternative is to choose microphone positions that satisfy the assumptions of the measurement, then regress the measurement surface to the microphone positions. Ellipsoidal sound power measurement surfaces offer good flexibility to choose microphone positions that satisfy the assumptions of the measurement and have available regression methodologies.

The ellipsoidal measurement surface provides a simpler test setup and several other advantages. A simple arrangement with as few as three microphones can be set up to support survey grade measurements; if better accuracy is desired more microphone positions can be added.

These characteristics in a hypothetical measurement surface would be beneficial:

[1] EZechmann@cdc.gov

1. Smooth, with no discontinuities.
2. Adjustable with three independent axes of contraction and dilation.
    a. Optimally satisfy the conditions of the far field, background noise, and environmental reflections.
    b. Adapt to the shape of the noise source as needed.
3. Available regression methods to fit the measurement surface to the microphone positions.
4. A systematic estimation of the cosine angle error due to a lack of a common normal vector between the measurement surface and reference surface.
5. A systematic estimation of the microphone directivity error due to pointing the free-field microphones in the direction of the center of the measurement surface.
6. A systematic estimation of the microphone position error—the relative difference between measured microphone position and the theoretical microphone position on the measurement surface.
7. A 3-microphone position sound power measurement with zero, one, two, or three orthogonal reflecting planes.
8. Be well-known, understood, and standardizable.

This paper covers the theory and tests the adequacy of ellipsoidal measurement surfaces. Section 2 of this paper describes the theory and three new corrections. Section 3 introduces theoretical measurement procedures. Sections 4 and 5 explain the methods and results for plotting, comparing, and analyzing measurement surfaces in ISO 3744 and 3745. Measurement surfaces are compared using simulated K_2 corrections for environmental reflections. Additional comparative analysis tools are graphically illustrated using a radiation behavior map and a microphone directivity correction plot.

2. BACKGROUND ON ELLIPSOIDS, THREE CORRECTIONS, AND SOUND FIELDS

Ellipsoids have several properties that are useful for implementing a simpler setup, however there is a tradeoff with the complexity of the calculations. The simpler setup is optimized to place the microphones approximately on the surface of an ellipsoid in the free-field and avoid the nearfield of the Device Under Test (DUT) and reflecting planes. The microphones are pointed at the center of the ellipsoid. This simpler setup requires the surface area associated with each microphone and three corrections at each microphone position to be calculated.

2.1 Geometric Assumptions

Consider an ellipsoid centered at the origin x=0, y=0, z=0. An aligned ellipsoid means that the cardinal radii are aligned with the axes of the coordinate system so that the radii (a, b, c) are aligned with rectangular axes (X, Y, Z). All ellipsoids in this article are assumed to be centered and aligned with the coordinate axes.

The reference surface must completely enclose the DUT. The measurement surface should be in the acoustical and geometrical farfield of the DUT. The measurement surface should be in the acoustical farfield of all reflecting planes. Optimally the reference and measurement surfaces should be parallel [5]. A spherical reference and measurement surfaces with a common center are true parallel surfaces. Ellipsoidal reference and measurement surfaces can only approximate parallel surfaces. Ellipsoids are promising as a better approximation of parallel surfaces than cylinders and parallelepipeds. Ellipsoids have three radii for adjusting the surface, are smooth, can be determined by as few as three microphone positions, and are well-known, understood, and standardizable.

2.2 Three Corrections

In this paper, regression methods specifying only centered aligned ellipsoids are used [6,7]. An ellipsoidal measurement surface is fit to the microphone positions. The surface area associated with each microphone position can be calculated using a nearest neighbor approach based on geodesics and numerical integration [6,8,9]. The deviation of the microphone positions from the measurement surface relative to the reference surface gives rise to a Microphone Placement Correction, L_{mpc} [6]. The deviation from the measurement surface is based on the shortest distance from a point to the

surface of an ellipsoid [10]. The angular misalignment of the normal vectors of the reference surface and measurement surface results in a cosine theta error correction (Normal Vector Misalignment Correction) L_{nvmc} [6,11,12]. Pointing the microphones at the center of the ellipsoid causes a microphone directivity error which is corrected using a Microphone Directivity Correction, L_{mdc} [13]. The surface areas associated with each microphone position and the three corrections L_{mdc}, L_{nvmc}, L_{mpc} are applied to all of the simulations in this paper.

2.3 Sound Fields

Figure 1 illustrates several acoustical field terms associated with sound power and sound energy measurements for a DUT with small compactness, kd_O. Compactness is the wavenumber multiplied by the characteristic distance and in part determines the radiation behavior of a source. Sound pressure levels can fluctuate dramatically in the near field of a source and the nearfield of large reflecting surfaces (walls and the ceiling). Consequently, sound pressure level measurements should be avoided in the nearfield of the DUT and large reflecting surfaces. For small compactness DUTs, free field measurements are made at least one-quarter wavelength away from the surface of the DUT.

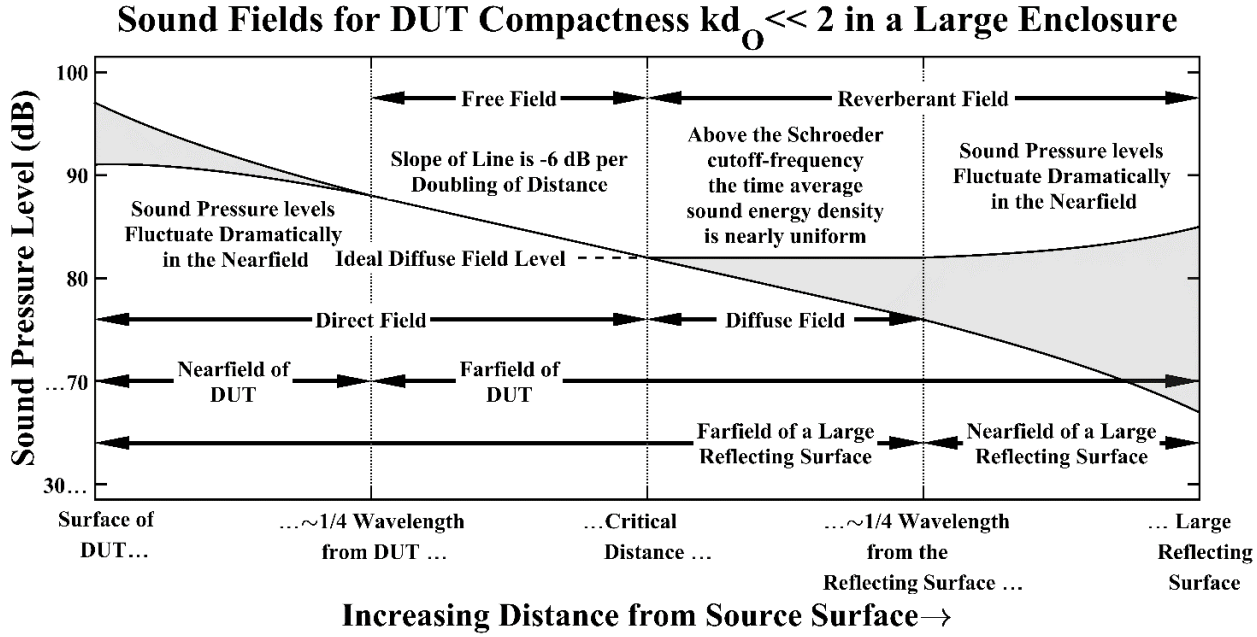

Figure 1: The sound fields for a sound energy measurement from nearfield at the source to the nearfield at a large reflecting surface such as a wall. The diffuse field is use for reverberation chamber sound energy measurements. The free field is used for hemi-anechoic chamber measurements.

3. THEORETICAL MEASUREMENT PROCESS AND SURVEY PROCEDURE

This section describes a theoretical process for making a sound power or sound energy measurement. The measurement process is supplemented with a survey procedure to estimate a single number metric.

3.1 Theoretical process for a sound power or sound energy measurement

The steps below are for a sound power or sound energy measurement made in a free field over a reflecting surface under hemi-anechoic conditions with the possibility of large reflecting surfaces (walls and ceiling). Note: steps 5-13 can be automated using computer programs.

1. Determine the x, y, z coordinates relative to a point directly below the center of the DUT.
2. Position the DUT over a reflecting plane.
3. Determine an enclosing reference ellipsoid for the DUT.
    a. Assume a centered aligned ellipsoid
    b. The maximum height of the reference ellipsoid at the top dead center point and a corner of a work bench-assuming symmetry can determine an ellipsoid.
    c. The program reference_ellipsoid.m [6] has more details.

d. The radii of the refence surface are denoted by (a_r, b_r, c_r).

4. Estimate d_O, the characteristic dimension of the DUT. This is the maximum length dimension across the DUT.
5. Estimate the frequencies of interest (one-third-octave bands from 125 Hz to 20 kHz)
   a. Estimate the lowest frequency of interest, F_{min}
6. Estimate the compactness of the source at F_{min}, $kd_O=d_O 2\pi F_{min}/c$
   a. c is the speed of sound ≈343 m/s
   b. For small equipment such as power tools
      compactness at F_{min} is often small, $kd_O << 2$
   c. For large equipment such as bull dozer or jumbo drill
      compactness at F_{min} is often large, $kd_O >> 2$
7. Estimate the distance to the acoustic farfield of the DUT.
   a. $d_{DUT,acoustic}=N_{DUT,wl}\times c/F_{min}$
      $N_{DUT,wl}$ is the Number of Wavelengths.
      Selecting the value of $N_{DUT,wl}$ is a complicated task that may require an experimental investigation of the sound field [3,14]. Table 1 shows rough estimates of the needed values.

Table 1: Compactness regimes for determining the acoustic farfield

DUT Compactness at F_{min} typically 125 Hz Regimes		Number of Wavelengths $N_{DUT,wl}$	Wavelength at 125 Hz (meters)
Small	$kd_O \ll 2$	1/4	0.7
Transition	$kd_O \sim 2$	1	2.7
Large	$kd_O \gg 2$	2	5.5

A piecewise function smooths the scaling $N_{DUT,wl}$ in terms of DUT compactness kd_O,

$$N_{DUT,wl} = \begin{cases} 1/4 & kd_O < 1 \\ 3/4\, kd_O - 1/2, & 1 \le kd_O < 2 \\ kd_O/2\,, & 2 \le kd_O < 4 \\ 2, & 4 \le kd_O \end{cases}. \quad (1)$$

   b. Wavelength at 125 Hz: $\lambda = \frac{c}{f} = \frac{343\ m/s}{125\ Hz} \approx 2.7$ m
   c. For a DUT with large compactness $kd_O \gg 2$, select $N_{DUT,wl} \sim 2$
   d. ISO 3745 requires $N_{DUT,wl} \ge 1/4$
8. Estimate the distance to the geometric farfield boundary.
   a. $N_{DUT,dO}$ is the multiplier for d_O to be in the geometric farfield of the noise source. Typically, $N_{DUT,dO} \sim 2$
   b. $d_{DUT,geometric}= N_{dO}\times d_O$
9. Estimate the maximum distance of the acoustic and geometric distance requirements.
   a. $d_{DUT,max}$=Maximum($d_{DUT,acoustic}$, $d_{DUT,geometric}$)
10. Calculate the acoustic and geometric requirements due to the limitations of the room size. Assume that the boundaries of a hemi-anechoic chamber are somewhat reflective at F_{min} and that staying a certain distance from the reflecting surfaces is a best practice.
    a. Acoustic Requirement: Stay at least one-quarter of a wavelength from reflecting surfaces. $N_{LRS,wl} \sim 1/4$
    b. $d_{LRS,acoustic} = N_{LRS,wl}\times c/F_{min}$
    c. Geometric Requirement: Stay at least 0.5 m from large reflecting surfaces
    d. $d_{LRS,geometric}$ =0.5 meters
       The subscript LRS is an abbreviation for Large Reflecting Surface (LRS).
11. Estimate the maximum distance of the acoustic and geometric distance requirements.
    a. $d_{LRS,max}$=Maximum($d_{LRS,acoustic}$, $d_{LRS,geometric}$)

12. Choose a "Pattern of Microphone Positions" based on appropriate standards such as ISO 3744, ISO 3745, and ANSI S12.15 [2-4]. These standards specify microphone positions whose spherical angular patterns can be projected onto a surface. Projecting an angular pattern leads to the figure of speech, "Pattern of Microphone Positions."
13. Select microphone positions at a distance $d_{DUT,max}$ normal to the reference surface with due consideration of the pattern of microphone positions and that are sufficiently far from large reflecting surfaces.
    a. For a survey grade measurement use a piece of string and good judgement such that the microphone positions have different heights and the microphone positions "look" like they will fit an ellipsoid and represent equal surface areas. Microphone positions with lower values of x and y should have greater values of z. Adjust the microphone positions away from reflecting surfaces and other obstacles. Satisfying the measurement assumptions is the goal.
    b. For a computer simulation, mathematically construct microphone positions on an ellipsoid with radii $(a_m, b_m, c_m) = (a_r, b_r, c_r) + d_{DUT,max}$. In this paper, the rectangular coordinate triple is transformed from the original spherical surface to an ellipsoidal surface while preserving the spherical angles (θ, ϕ). Those angles are then input directly into the Gauss parametric form (a, b, c, θ, ϕ) [15]. This causes a reasonable spread of the microphone positions along the surface. After the surface is constructed, the ellipsoid is scaled to satisfy the room size requirements.
14. If the microphone positions cannot satisfy the requirements due to room size increase the minimum frequency or find a larger space to conduct the measures. If the microphone positions are too close to the source, then move them further away from the source. If the microphone positions do not represent equal areas nudge them in a direction that looks like they will better represent equal areas.
15. Iterate steps 12-14 until an acceptable set of microphone positions has been identified.
16. Measure and record the x, y, z coordinates of the microphones preferably within 1 cm.
17. Verify that the Recorded Microphone Positions are likely to produce successful results. Run simulations of the K_2 values for the selected microphone positions by entering the coordinates and other information into ms_interference_monopole.m or ms_interference_oscillating_sphere.m [6].

3.2 Theoretical survey procedure for estimating a single number metric

This procedure starts after the successful completion of the procedure from Section 3.1. This article only simulates this procedure. The calculations were verified with sample data [6,16].

1) Use the procedure from Section 3.1 to setup the DUT and microphones.
2) Make sound pressure level measurements of the Background Noise, Reference Sound Source (RSS), and DUT at the microphone positions
    a. Use fractional octave bands if possible
    b. For sound energy measurements, carefully keep track of the elapsed time
3) Enter data into a program such as LW_LJ_estimate_dut_bg_rss4.m [6].
4) Check if the K_1 and K_2 values are acceptable. Find a different measurement location if needed. K_1 is the correction for background noise.
5) Check the directivity index of the results and add more microphone positions as needed.

4. METHODS

The measurement surfaces from ISO 3745 and ISO 3744 are commonly used for sound power measurements (see Table 2). These surfaces were tested using a 2-meter radius and with an optimized ellipsoid. Duplicate microphone positions were removed. The optimized ellipsoid had the smallest ellipsoidal radii satisfying the acoustic and geometric farfield conditions at 125 Hz. The microphone positions in the optimized measurement surfaces were determined by transforming the original spherical angles to the ellipsoidal angles in the Gauss parametric form as described in step 13b in Section

3.1. Table 2 describes the measurement surface properties that were used in the simulations. For the measurement surfaces using traverses, the number of microphone positions ranged from 48 to 120.

Table 2: Properties of ISO 3745 and ISO 3744 measurement surfaces

Standard	Table	Figure	Description	Number of Reflecting Planes	Number of Microphone Positions
ISO 3745	D1	-	Sphere	0	40
ISO 3745	E1	-	Hemisphere	1	40
ISO 3745	E2	-	Hemisphere	1	40
ISO 3745	-	F1	Hemisphere	1	120
ISO 3745	-	G1	Hemisphere	1	48
ISO 3745	-	H1	Hemisphere	1	100
ISO 3744	B1	-	Hemisphere	1	20
ISO 3744	B2	-	Hemisphere	1	19
ISO 3744	B2	-	Hemisphere	1	10
ISO 3744	B2	-	One-Fourth Sphere	2	9
ISO 3744	B2	-	Hemisphere	1	6
ISO 3744	B3	-	One-Eight Sphere	3	5
ISO 3744	F1	-	Hemisphere	1	12
ISO 3744	F1	-	Hemisphere	1	6
ISO 3744	-	B5	Hemisphere	1	60
ISO 3744	B2	-	One-Half Ellipsoid	1	19
ISO 3744	B2	-	One-Half Ellipsoid	1	10
ISO 3744	F1	-	One-Half Ellipsoid	1	12

In two separate sets of simulations, the DUT was simulated using monopoles (pulsating spheres) and dipoles (oscillating spheres). The compactness of the simulated DUT had three levels: small, transition, and large. Table 3 shows the compactness values and diameters of the monopole and dipole sources used to model the DUTs. The sources were in a hypothetical cube shaped box with edges of length 0.3 meters. The simulations were run with three distinct heights of the hypothetical box 0.01, 0.3 and 1 (m) above the plane z=0. The centers of the sources were located in a cube shaped box and always on the positive side of any abutting reflecting planes. The source height and hypothetical box dimension were used to determine the reference surface and geometric farfield. The source positions, frequencies within each one-third-octave band, phases, diameters, and acoustic velocities, were selected at random from a uniform distribution. One-third-octave bands from 125 Hz to 20 kHz were used. Each sound power simulation was averaged over 1,000 runs with 2,000 sources.

Table 3: DUT Compactness at 1 kHz, mean and standard deviation (Std) of the source diameter.

Compactness at 1 kHz	Mean(d_O) (m)	Std(d_O) (m)	Local Wave propagation	Radiation efficiency
Small ($kd_O = 0.19$)	0.0136	0.00200	Spherical	Low
Transition ($kd_O = 1.9$)	0.136	0.0200	Spherical to Planar	Low to High
Large ($kd_O = 19$)	1.36	0.200	Planar	High

In a similar way, a toss of a piezo football—battery powered piezoelectric buzzer inside a foam ball—in a parabolic arc was simulated [17]. The simulated piezo football toss had a symmetric parabolic trajectory going from (0.5, 10, 2.5) through top center (0, 0, 3) m to (-0.5, -10, 2.5).

K_2 values were estimated for each simulation by calculating the difference between the theoretical sound power and the sound power estimated from the sound pressure at the microphone positions [18-20]. The theoretical sound power was corrected for the influence of reflecting surfaces [21,22]. Maps of the radiation behavior were made using the characteristic dimension of the sources to better understand if the sources were in the farfield, hydrodynamic nearfield, geometric nearfield, or a transition among those fields [14].

5. RESULTS

This shows examples of the surface mappings of microphone positions, DUT radiation behavior maps, the sound power frequency profiles for the three levels of DUT compactness, simulated K_2 corrections for environmental reflections, and microphone directivity corrections.

5.1 Surface mapping of microphone positions

Figures 2 and 3 show the surface mapping for a selection of ISO 3745 and 3744 surfaces resepctively. Selected microphone positions are marked with a grey disk and numbered. Figure 4 shows a comparison of the 2-meter radius hemisphere and an optimized smallest radii ellipsoid.

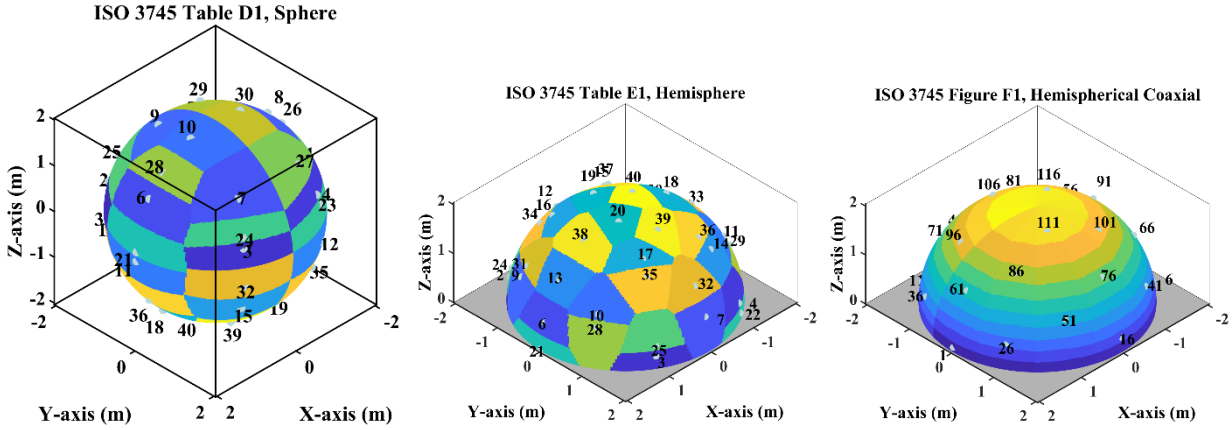

Figure 2: Mapping of ISO 3745 microphone positions on a 2-meter radius to the nearest surface areas.

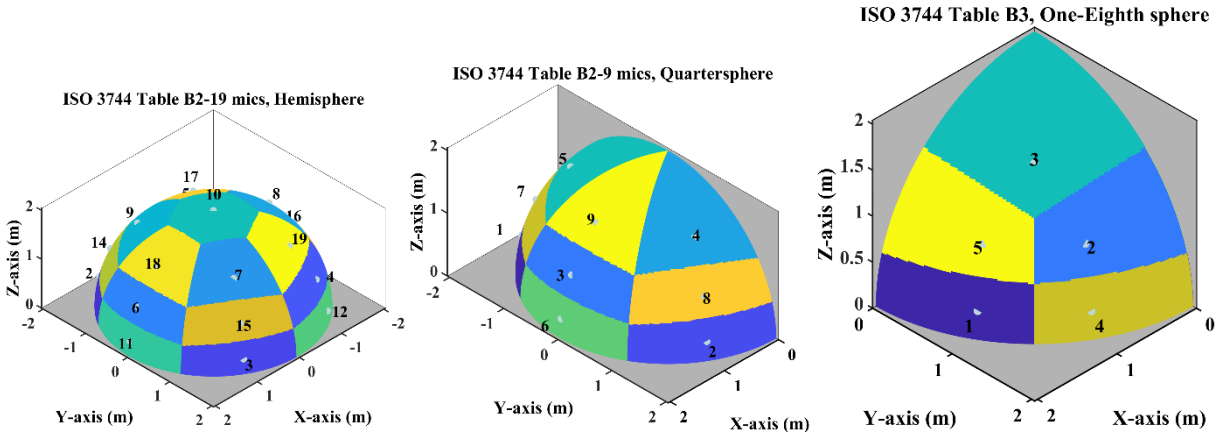

Figure 3: Mapping of ISO 3744 microphone positions to the nearest surface area.

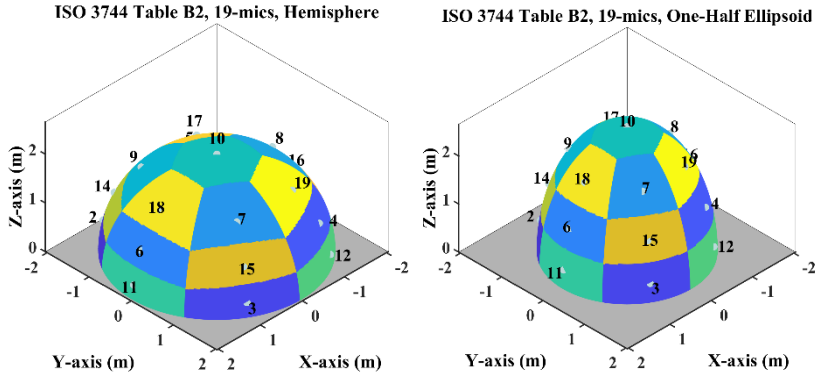

Figure 4: Comparison a 2-meter radius hemisphere to an optimized ellipsoid with radii (1.6, 1.6, 2.6) m. The optimized ellipsoid more closely conforms to the shape of the DUT.

Figure 5 shows the surface area to microphone position mapping for the piezo football toss simulation with 19 microphone positions. In Figure 5, the left plot uses the prechosen radii of (20, 6,

5) m and the right plot uses radii optimized to satisfy the conditions of the acoustic farfield at 125 Hz and geometric farfield with a characteristic dimension of 0.25 m.

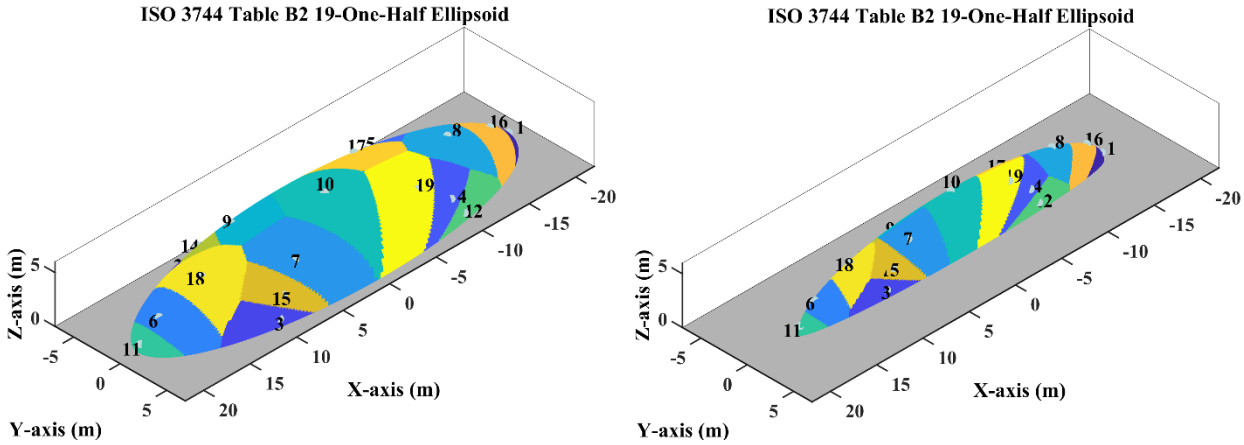

Figure 5: Mapping of piezo football toss simulation with 19 microphone positions based on Table B2 with removal of the duplicate microphone position. The left plot uses the prechosen radii of (20, 6, 5) m. The plot on the right uses the optimized smallest radii to satisfy the conditions of the acoustic farfield at 125 Hz and geometric farfield with a characteristic dimension of 0.25 m.

5.2 DUT radiation behavior map

Figure 6 shows a DUT radiation behavior map for the piezo football toss setup with radii (20, 6, 5) m using the d_O from Table 3. Ideally all of the markers (**x**, **o**, **+**) would be in the farfield and not in the hydrodynamic nearfield. As the measurement surface radii increase the markers shift towards increasing geometric ratio, G-values and towards the farfield. As the frequency increases the markers shift toward increasing compactness, C-values and the geometric nearfield.

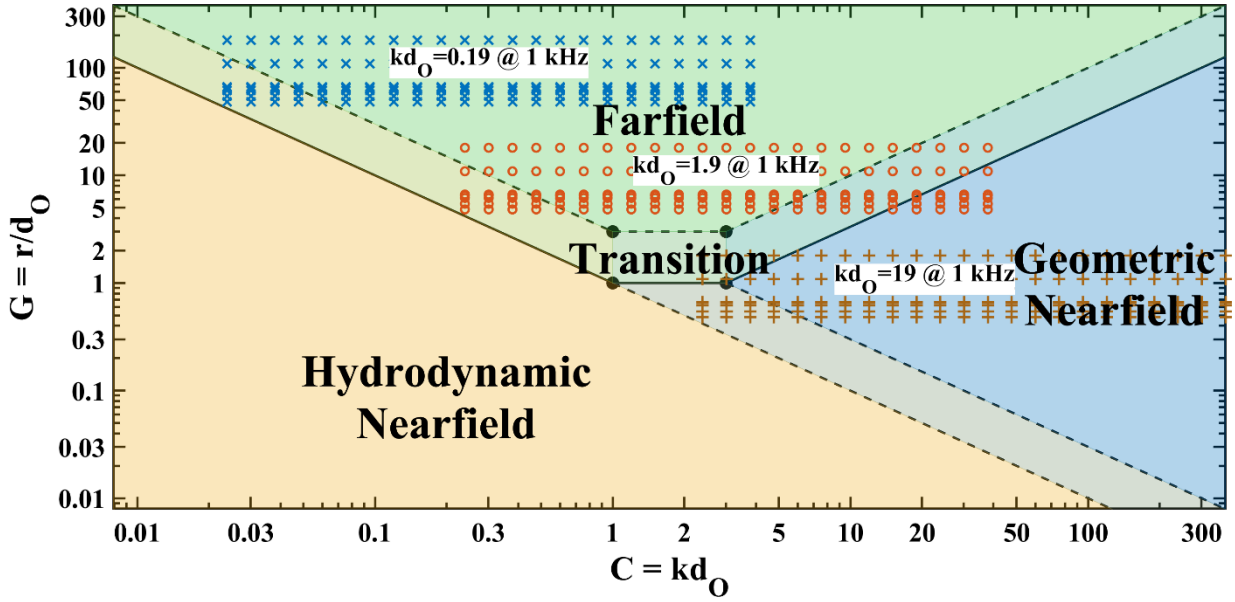

Figure 6: DUT radiation behavior geometric ratio and compactness map of the piezo football toss setup using the ISO 3744 Table B2 19-microphone positions. Each marker represents a microphone position and frequency with **x**-small, **o**-transition, and **+**-large compactness, kd_O.

5.3 Sound power frequency profiles for small, transition, and large compactness

Figure 7 shows the shape of the sound power frequency profile for the three levels of compactness: small, transition, and large. For small compactness the sound power increases as the frequency increases. For large compactness the sound power is nearly constant as the frequency increases. All the simulations had similar shaped sound power frequency profiles.

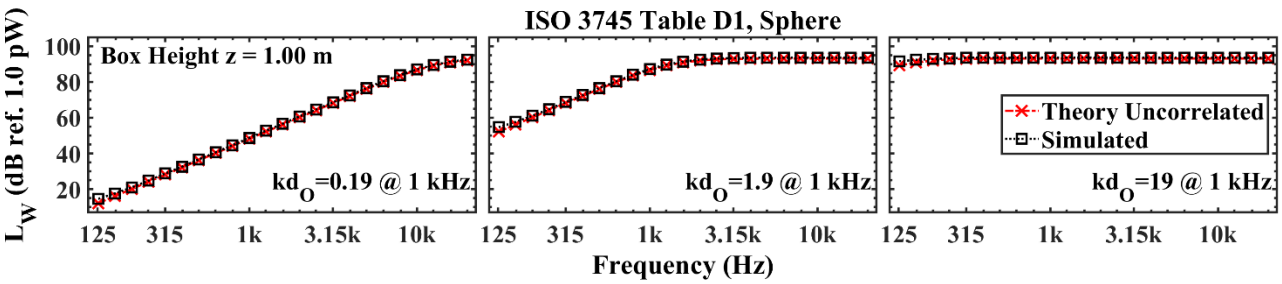

Figure 7: Sound power of uncorrelated monopole sources using a simulated ISO 3745 D1 40-microphone setup with small, transition and large compactness.

5.4 Simulated K_2 corrections for environmental reflections ISO 3744 and 3745 surfaces

Figure 8 shows the simulated K_2 values for oscillating sphere models with the optimized ellipsoidal radii. The K_2 values for the monopoles are closer to zero than for the oscillating sphere sources. In some cases the oscillating sphere model has much worse outcomes than the monopole model. K_2 values for the original spherical shapes are generally closer to zero than for the optimized ellipsoidal radii. The plots depict a worst case for the K_2 values given the models. For the simulations with zero and one reflecting planes, the K_2 values generally remain with ±2 dB with a few minor exceptions.

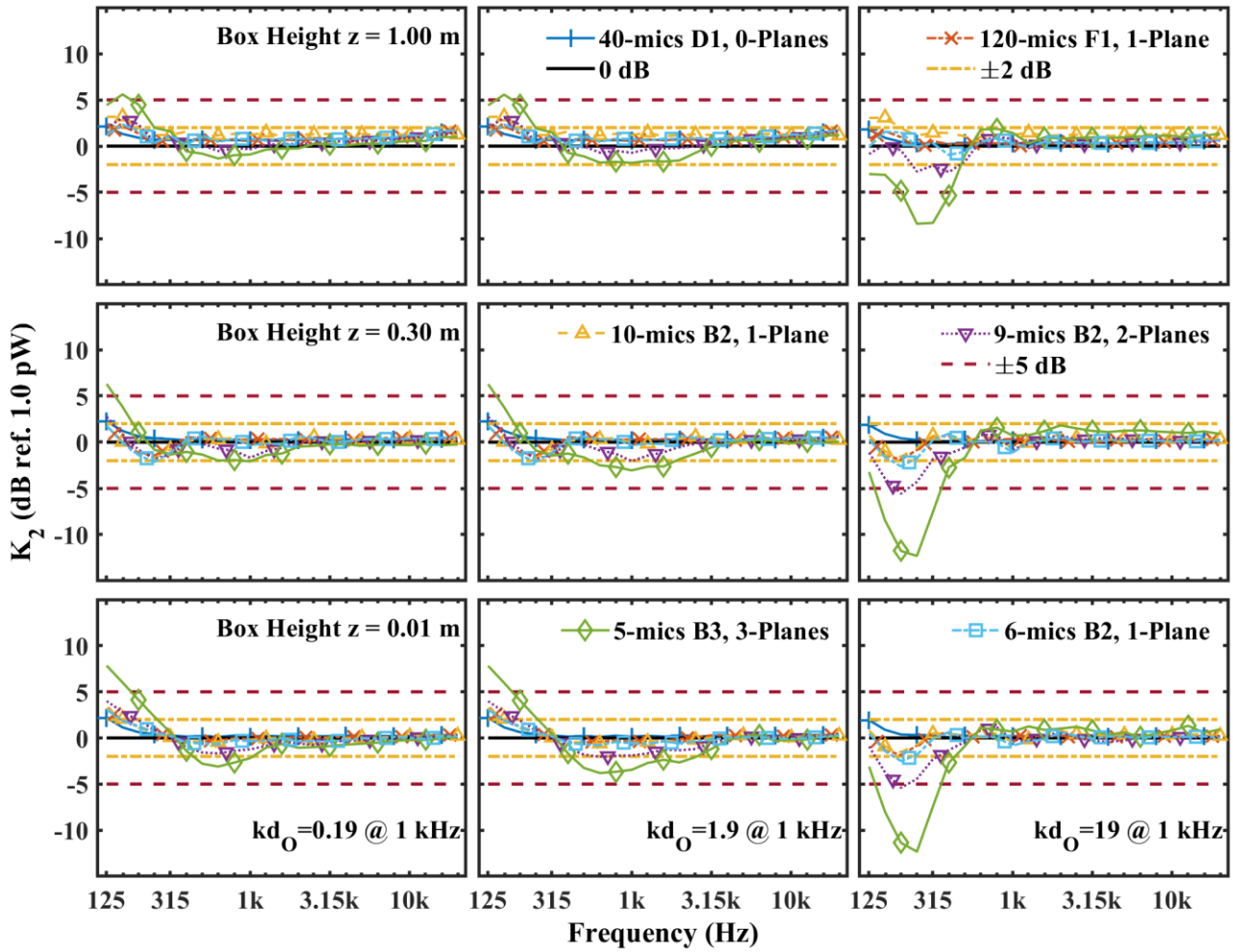

Figure 8: K_2 values for three source heights 0.01, 0.3, and 1.0 m and three levels of compactness: small, transition and large. The height and compactness increase along the rows and columns respectively. The plot legends indicate the number of microphones, table the measurement surface came from and the number of reflecting planes. As the number of reflecting planes increase, the K_2 values increasingly deviate from 0 dB.

5.5 Microphone directivity

Figure 9 plots the microphone directivity correction level, L_{mdc} for all microphone positions and frequencies for 11 measurement surfaces. The measurement surfaces and radii are identified in the plot legends. For the measurement surfaces that have equal radii, L_{mdc} is nearly zero from 315 Hz to 40 kHz. For the optimized measurment surfaces (OMS) that have increasingly unequal radii the L_{mdc} is increasingly large. Measurement surfaces should be chosen with the aim of keeping the radii sufficiently equal to keep L_{mdc} sufficiently small.

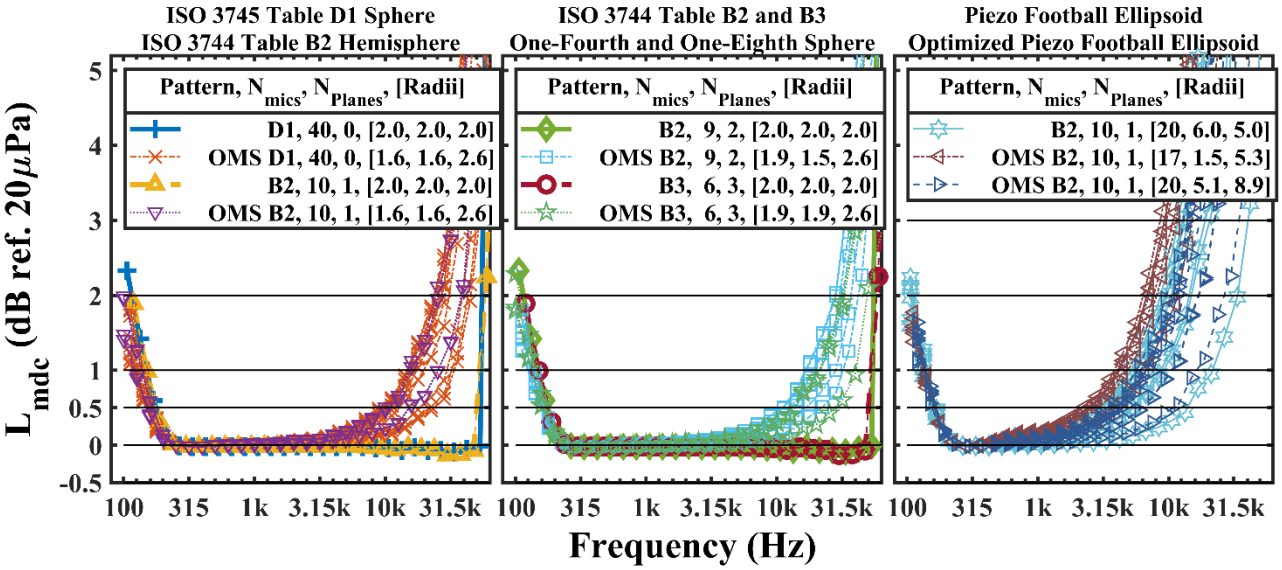

Figure 9: Microphone directivity correction level for all microphone positions for the selected measurement surfaces. As the ellipsoidal radii increasingly deviate from equality L_{mdc} increases especially above 5 kHz. Measurement surfaces should be chosen with keeping L_{mdc} relatively small.

5.6 Simulated K_2 corrections for piezo football toss

Figure 10 shows that the simulated K_2 value of the piezo football toss is much higher than for the simulations that had nearly equal radii. The deviation of the radii from being nearly equal increased the microphone directivity correction at frequencies above 5 kHz as shown in Fig. 9. The increase in L_{mdc} resulted in an increased simulated K_2 correction for environmental reflections.

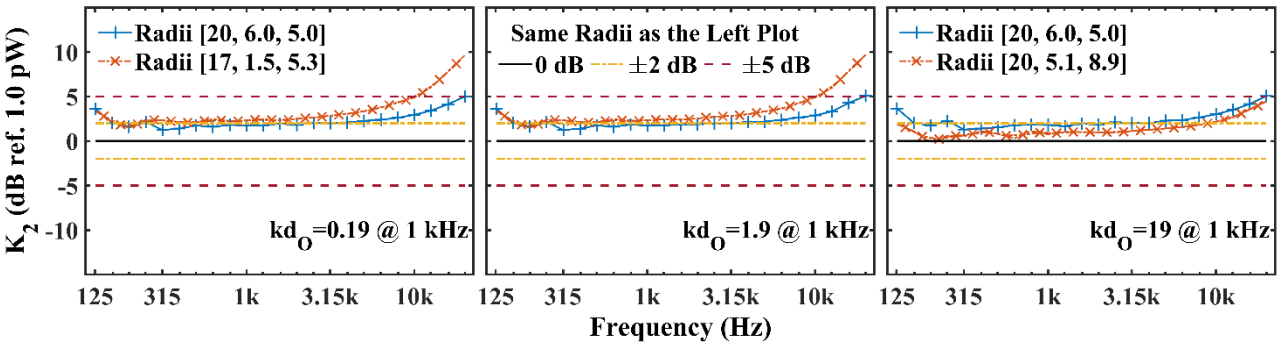

Figure 10: K_2 values for the piezo football toss with three levels of compactness: small, transition and large. K_2 values increasingly deviate from 0 dB as the frequency increases because the microphone directivity correction level dominates as the radii increasingly deviate from equality.

6. CONCLUSIONS

Measurement positions in ISO 3745 and ISO 3744 with zero or one reflecting planes generally had simulated K_2 values satisfying $-2 < K_2 < +2$ dB. That was generally observed for all of the simulations

with the small, transition, and large compactness sources with monopole and oscillating sphere models. The optimized ellipsoidal measurement surfaces also satisfied these conditions for the measurement surfaces that had less than three reflecting planes and close to equal radii. For the simulations of the measurement surface with two or three reflecting planes, the K_2 values at different heights and compactness regimes were outside of the range of $-2 < K_2 < +2$ dB. In general, as the number of reflecting planes increased the K_2 values increasingly deviated from 0 dB. Measurements near two or three reflecting planes may be inaccurate and should be avoided. For the piezo football toss, optimizing the radii of the measurement surfaces to be small, does not yield the best simulated K_2 values. Keeping the radii of the measurement surfaces reasonably close to equal seems to yield simulated K_2 values closer to 0 dB. Plots of the simulated K_2 values, radiation behavior maps, and microphone directivity correction levels will likely help to assess whether the measurement surface satisfies the assumptions of the sound power measurement.

7. FUTURE WORK

This paper briefly outlined the theory and possible practical applications of sound power measurements using the ellipsoidal measurement surface. A more complete description of theory and experimental results are needed to better understand the methodology. The simulated K_2 corrections presented in this paper need to be compared to experimental estimates of K_2 corrections to better understand the accuracy of this method.

Further development of this methodology may help to answer some research questions. For a DUT with a high directivity factor, what is the best strategy for adding additional microphone positions to improve accuracy and reduce uncertainty of the sound power estimate? How can the methodology be practically implemented in field measurements using the microphone positions described in ISO 3746:2010 Section 8.2 [23]. How can K_2 corrections be estimated in a more accurate, reliable, and cost-effective way [24-28]. Does the free-field ellipsoidal sound power measurement have an analogous measurement in the diffuse field [29-30]. How can sound energy measurements be incorporated into a “Buy Quiet” strategy with a more holistic approach considering all health, safety, and cost factors influencing purchasing decisions? How would the safety procurement standard SAE AS6228 benefit from sound energy measurements using the ellipsoidal measurement surface [1]?

8. REFERENCES

1. SAE AS6228, (2014). Safety Requirements for Procurement, Maintenance and Use of Hand-held Powered Tools, United States of America, Warrendale, PA. SAE international, Retrieved 2015/10/27, from https://www.sae.org/standards/content/as6228/
2. ISO 3744 (2010). Acoustics — Determination of sound power levels and sound energy levels of noise sources using sound pressure — Engineering methods for an essentially free field over a reflecting plane, International Organization for Standardization, Geneva, Switzerland
3. ISO 3745 (2010). Acoustics — Determination of sound power levels and sound energy levels of noise sources using sound pressure — Precision methods for anechoic rooms and hemi-anechoic rooms, International Organization for Standardization, Geneva, Switzerland
4. ANSI S12.15 (1992). Acoustics–portable electric power tools, stationary and fixed electric power tools, and gardening appliances–Measurement of sound emitted, American National Standards Institute, Acoustical Society of America, New York, (1992).
5. Sabitov, I.Kh. (2020). *Parallel surfaces*, Encyclopedia of Mathematics, (Accessed 27 November 2020). https://bit.ly/2Isa6Kh
6. Zechmann, E. (2021). Ellipsoidal Sound Power Measurement Surface, MATLAB Central File Exchange. (Accessed 2 April 2021). (https://bit.ly/3fyOKaQ)
7. Petrov, Y. (2020) *Ellipsoid fit*, MATLAB Central File Exchange, (Accessed 22 September 2020). https://bit.ly/3qy70FX,
8. Poelaert, D., Schniewind, J., & Janssens, F. (2011). Surface Area and Curvature of the general Ellipsoid. (Accessed 24 August 2020) https://arxiv.org/pdf/1104.5145.

9. Panou, G., & Korakitis, R. (2019). Geodesic equations and their numerical solution in Cartesian coordinates on a triaxial ellipsoid. Journal of Geodetic Science, 9(1), 1-12.
10. Eberly, D. (2020), *Least squares fitting of data by Linear or Quadratic Structures*, Geometric Tools, Redmond, WA: (Accessed 11 December 2020). https://bit.ly/3jQOyVS,
11. Nobile, M. A., Fiore, F., & Boyes, R. N. (2006). Measurement of sound power level using enveloping surfaces: Investigation of the cos (θ) error. Proceedings of Inter-noise (2006) 4, 3411–3420
12. Probst, W. (1999). Checking of sound emission values. Wirtschaftsverl. NW, NW, Bremerhaven, Bremen, Germany pp. 28–34
13. PCB Piezotronics, (2020). *Understanding sound power and microphone response: A complete guide to acoustic fundamentals*, (Accessed 8 October 2020) https://bit.ly/37ICalj, p. 12.
14. Hansen, C. H. (2005). Noise control: from concept to application. Taylor and Francis. New York, p 127-129
15. Bektas, S. (2017). Curvature of the Ellipsoid with Cartesian Coordinates. Landscape Architecture and Regional Planning, 2(2), 61-66.
16. NIOSH power tools dataset (2009). Retrieved 2021/01/21 from https://www.cdc.gov/niosh/topics/noise/pdfs/Tool_Test_Noise_Summary.xlsx
17. Gabrielson, T. B. (2014, September). Building on the foundations of acoustics through demonstrations. In INTER-NOISE and NOISE-CON Congress and Conference Proceedings (Vol. 248, No. 1, pp. 648-655). Institute of Noise Control Engineering.
18. Ansol Coustyx, (2007). *Pulsating sphere: Demo of indirect boundary element models*, Advanced Numerical Solutions LLC, https://bit.ly/3lQYTAE, (Accessed 5 October 2020), Eqns. 1, 8.
19. Chanaud, R. C. (2010). Tools for analyzing sound sources, CCR Associates, LLC, Essex, Connecticut, (Accessed 21 May 2021), https://bit.ly/3ucz4PA, pp. 3-9, 3-12, Eqns. 3.16, 3.20.
20. Ansol Coutyx, (2008). *Oscillating sphere: Demo of indirect boundary element models*, Advanced Numerical Solutions LLC, (Accessed 5 October 2020), https://bit.ly/2IsA3tl, Eqns. 1, 11.
21. Ingard, U., & Lamb Jr, G. L. (1957). Effect of a reflecting plane on the power output of sound sources. The Journal of the Acoustical Society of America, 29(6), 743-744.
22. Bies, D. A. (1961). Effect of a reflecting plane on an arbitrarily oriented multipole. The Journal of the Acoustical Society of America, 33(3), 286-288.
23. ISO 3746 (2010). Acoustics — Determination of sound power levels and sound energy levels of noise sources using sound pressure — Survey method using an enveloping measurement surface over a reflecting plane, International Organization for Standardization, Geneva, Switzerland
24. Hubner, G. (2010, June). Some actual problems and solutions standardazing sound power measurements. In INTER-NOISE and NOISE-CON Congress and Conference Proceedings (Vol. 2010, No. 8, pp. 3078-3087). Institute of Noise Control Engineering.
25. Kurtz, P. (2010, June). Sound power measurements according ISO 3744-Some unsolved problems. In INTER-NOISE and NOISE-CON Congress and Conference Proceedings (Vol. 2010, No. 7, pp. 3639-3648). Institute of Noise Control Engineering.
26. Sgrieß, D., Picker, K., & Wittstock, V. (2021). Investigation on a possible future qualification of free field environments with impulse methods, Acoustics in Practice®. https://bit.ly/37rvqZO
27. Heisterkamp, F., & Arendt, I. (2018, December). Simplified Determination Of the Environmental Correction For Noise Emission Measurements. In INTER-NOISE and NOISE-CON Congress and Conference Proceedings (Vol. 258, No. 6, pp. 1286-1295). Institute of Noise Control Engineering.
28. Johnson Sr, R. S., & Brittain, F. H. (2013, August). An empirical method to improve accuracy of in-situ sound power measurements of industrial equipment. In INTER-NOISE and NOISE-CON Congress and Conference Proceedings (Vol. 246, No. 1, pp. 510-519). Institute of Noise Control Engineering.
29. ISO 3741 (2010). Acoustics — Determination of sound power levels and sound energy levels of noise sources using sound pressure — Precision methods for reverberation test rooms, International Organization for Standardization, Geneva, Switzerland
30. Hodgson, M. (1996). When is diffuse-field theory applicable? Applied Acoustics, 49(3), 197-207.